communications biology

A Nature Portfolio journal

Article

https://doi.org/10.1038/s42003-025-07839-w

Peli1, regulated by m^{6}A modification, suppresses NLRP3 inflammasome activation in atherosclerosis by inhibiting YB-1

Qiang Liu[1,2,4], Lu Yan[1,4], Tao Wu[1], Qinghua Wu[1], Ben Ke[3] ✉ & Wen Shen[1] ✉

The activation of pyrin domain-containing-3 (NLRP3) inflammasome in macrophages is a risk factor accelerating the progression of atherosclerosis (AS). Here, the function of pellino 1 (Peli1) in regulating the activation of NLRP3 inflammasome during the development of AS was investigated. Our results showed that Y-box binding protein 1 (YB-1) knockdown could inhibit the progression of AS in vivo, and YB-1 silencing repressed oxidized low-density lipoprotein (ox-LDL)-mediated lipid accumulation and inflammation in macrophages by inactivating NLRP3 inflammasome. E3 ubiquitination ligase Peli1 mediated ubiquitination-dependent degradation of YB-1 during AS progression. Moreover, it was found that YTH domain-containing 2 (YTHDC2) recognized methyltransferase-like 3 (METTL3)-mediated Peli1 N6-methyladenosine (m^{6}A) modification and mediated Peli1 mRNA degradation. Rescue studies revealed that YB-1 upregulation abrogated the repressive effect of Peli1 upregulation on AS progression both in vitro and in vivo. Taken together, Peli1, regulated by m^{6}A modification, inhibited YB-1-mediated activation of NLRP3 inflammasome in macrophages by promoting YB-1 ubiquitination to suppress the progression of AS.

Atherosclerosis (AS) is an inflammatory disease driven by the accumulation of cholesterol-rich macrophages ("foam cells") in the arterial walls[1], which is the main cause of coronary heart disease and cerebral infarction[2]. The current therapeutic methods for AS include lipid-lowering and vasodilator medications, although these therapies cannot directly address atherosclerotic lesions[3]. Therefore, therapeutic strategies targeting AS are urgently needed, and the pathogenesis of AS must be elucidated to achieve the goal. The nucleotide-binding domain, leucine-rich-containing family, pyrin domain-containing-3 (NLRP3) inflammasome, a cytosolic protein complex whose basic structure is NLR (receptor), ASC (adaptor) and caspase 1 (effector)[4], can be activated by cholesterol crystals[5]. The activation of NLRP3 inflammasome in macrophages results in interleukin (IL)-1β and IL-18 secretion and promotes the occurrence and development of AS[6]. Therefore, it's suggested that inactivation of NLRP3 inflammasome in macrophages may be an effective therapeutic strategy targeting AS.

Y-box binding protein 1 (YB-1), as a cold shock protein, regulates various biological processes by modulating target transcription and translation[7]. YB-1 has been frequently recognized as a candidate protein associated with inflammatory reactions and a possible therapeutic target for inflammatory diseases[8–10]. A recent work demonstrated the significance of YB-1 in AS, especially that silencing YB-1 decreased AS development by inhibiting vascular smooth muscle cell (VSMC) phenotypic switching[11]. Notably, it was previously reported that YB-1 inhibition contributed to NLRP3 inflammasome inactivation during acute liver failure progression[12]. Nevertheless, the role of YB-1 in mediating the activation of NLRP3 inflammasome in macrophages during AS development remains unknown and deserves further research.

Protein ubiquitination acts as a key role in regulating inflammatory responses[13]. E3 ubiquitin ligase Pellino 1 (Peli1) is an E3 ubiquitination ligase, which can mediate the ubiquitination of downstream targets and then regulate immune responses[14]. Interestingly, Peli1 regulates systemic and local vascular inflammation, and Peli1 deficiency enhances foam cell production, which promotes AS development[15]. Herein, by using bioinformatics prediction, it was found that YB1 is the potential substrate of Peli1.

[1]Department of Cardiovascular Medicine, The Second Affiliated Hospital, Jiangxi Medical College, Nanchang University, Nanchang, China. [2]Department of Cardiovascular Medicine, Jiangxi Provincial People's Hospital, The First Affiliated Hospital of Nanchang Medical College, Nanchang, China. [3]Department of Nephrology, The Second Affiliated Hospital, Jiangxi Medical College, Nanchang University, Nanchang, China. [4]These authors contributed equally: Qiang Liu, Lu Yan. ✉e-mail: keben-1989125@163.com; 18146622197@163.com

However, whether Peli1 regulates AS progression by mediating YB1 ubiquitination-dependent degradation has not been reported before.

N6-methyladenosine (m^6A) methylation is the most common internal RNA modification[16]. Abnormal changes of m^6A may result in dysregulation of downstream genes expression, affecting the inflammatory response, ultimately promoting AS progression[17,18]. The m^6A regulatory enzyme consists of m^6A methyltransferase ("writers"), m^6A binding protein ("readers"), and m^6A demethylase ("erasers"). RNA methyltransferase methyltransferase-like 3/14 (METTL3/14), as major m^6A writers, are involved in AS development via regulation of RNA m^6A level. For instance, Zheng et al. demonstrated that METTL14 expression was markedly increased in LPS-treated THP-1 cells and its knockdown markedly reduced macrophage inflammatory response by regulation of Myd88 m^6A modification[17]. Meanwhile, it was previously reported that METTL14 accelerated AS development by mediating FOXO1 m^6A modification[18]. Furthermore, Dong et al. discovered that METTL3 was significantly increased in oxidized low-density lipoprotein (ox-LDL)-treated HUVECs, and its silencing repressed cell proliferation, migration, tube formation and VEGF expression in ox-LDL-treated HUVECs[19]. Herein, by using bioinformatics prediction, it was found that there were potential m^6A modification sites on Peli1, and Peli1 expression was inversely related to the m^6A modification level. However, whether METTL3 mediates Peli1 m^6A modification to regulate Peli1 expression level in AS is unknown. The effect of m^6A on RNA stability is dependent on the m^6A reader. m^6A writer can cooperate with m^6A reader to regulate the methylation and translation of downstream targets. Herein, it was predicted that Peli1 was the target of m^6A reader YTH domain-containing 2 (YTHDC2). However, whether YTHDC2 regulates Peli1 level in AS in a METTL3-mediated m^6A modification-dependent manner has not been reported before.

It's speculated that Peli1, regulated by METTL3-YTHDC2-mediated m^6A modification, inhibits YB-1-mediated activation of NLRP3 inflammasome by promoting YB-1 ubiquitination to suppress AS progression. Our research provides a theoretical basis for developing potential therapeutic strategies for AS.

Results

YB-1 knockdown inhibited AS progression in vivo

YB-1 is a candidate protein closely related to inflammatory responses and is a potential therapeutic target for inflammatory diseases including AS[10,11]. To investigate the effects of YB-1 on AS progression in vivo, AS model mice were established, and YB-1 knockdown was induced. As revealed in Fig. 1A, a high-fat diet (HFD) markedly increased YB-1 protein level in the arterial tissues of Apolipoprotein E-deficient ($ApoE^{-/-}$) mice, which was abolished after YB-1 knockdown. In addition, HFD treatment increased plasma total cholesterol (TC), triglyceride (TG), high-density lipoprotein cholesterol (HDLC) and low-density lipoprotein cholesterol (LDLC) levels in $ApoE^{-/-}$ mice, whereas YB-1 knockdown increased plasma HDLC level and reduced plasma TC, TG and LDLC levels in HFD-treated $ApoE^{-/-}$ mice (Table 1). The results of histopathological analysis subsequently revealed that lipid accumulation in the whole artery was markedly increased by HFD, whereas this change was partially eliminated by YB-1 silencing (Fig. 1B). In addition, HFD resulted in lesions and increased lipid accumulation in arterial tissues of $ApoE^{-/-}$ mice, while YB-1 knockdown remarkably ameliorated pathological changes and lipid accumulation (Fig. 1C–E). Meanwhile, mice were injected with AAV-LysM-sh-YB-1 (which can specifically knock down YB-1 in myeloid cells) and fed with HFD for 12 weeks. The expression of YB-1 in macrophages (CD68-positive) was significantly reduced in the plaque tissues of the AAV-LysM-sh-YB-1 group (Supplementary Fig. 1A). YB-1 knockdown increased plasma HDLC level and reduced plasma TC, TG and LDLC levels (Supplementary Table 1). In addition, AAV-LysM-sh-YB-1 injection reduced lipid accumulation in the entire aortic plaque area and relieved the lesions and lipid accumulation in arterial tissues (Supplementary Fig. 1B–E). Collectively, YB-1 knockdown effectively prevented AS progression in vivo.

YB-1 promoted ox-LDL-induced lipid accumulation in macrophages by regulating NLRP3

Foam cell formation, induced by phagocytizing ox-LDL by macrophages in the early atherosclerotic plaques, is an important factor in AS progression[20]. Herein, Raw264.7 cells stimulated by ox-LDL were used as the AS cellular model, and it was found that ox-LDL upregulated YB-1 expression and nuclear localization in Raw264.7 cells (Fig. 2A). As previously reported, YB-1 inhibition contributed to NLRP3 inflammasome inactivation during acute liver failure progression[12]. Herein, as revealed by the Chromatin immunoprecipitation (ChIP) assay, YB-1 bound with NLRP3 promoter (Fig. 2B). Meanwhile, it also turned out that YB-1 overexpression increased the luciferase activity presented by NLRP3 promoter-wt but had no significant effect on that of NLRP3 promoter-mut (Fig. 2C), suggesting that YB-1 transcriptionally facilitated NLRP3 expression in Raw264.7 cells. YB-1 knockdown was subsequently induced in ox-LDL-treated Raw264.7 cells, and the result demonstrated that ox-LDL stimulation increased YB-1, NLRP3 and caspase-1 protein levels in Raw264.7 cells, whereas YB-1 knockdown reversed these effects (Fig. 2D). Secretion levels of IL-1β and IL-18 in Raw264.7 cells were increased by ox-LDL treatment, which was abolished by YB-1 knockdown (Fig. 2E). As shown in Fig. 2F, ox-LDL treatment increased protein levels of cleaved IL-1β and pro-IL-1β in Raw264.7 cells, while YB-1 knockdown significantly reduced their expression (Fig. 2F). Moreover, ox-LDL treatment increased lipid accumulation in Raw264.7 cells, while this effect of ox-LDL was reversed by YB-1 silencing (Fig. 2G). Raw264.7 cells were co-transfected with NLRP3-pcDNA3.1 and si-YB-1 and then subjected to ox-LDL treatment. It was observed that NLRP3 overexpression prevented si-YB-1-induced decrease in NLRP3 and caspase-1 protein levels (Supplementary Fig. 2A), secretion levels of IL-1β and IL-18 (Supplementary Fig. 2B), protein levels of cleaved IL-1β and pro-IL-1β (Supplementary Fig. 2C), and lipid accumulation (Supplementary Fig. 2D) in ox-LDL-treated Raw264.7 cells. Collectively, YB-1 knockdown repressed ox-LDL-mediated lipid accumulation in macrophages by targeting NLRP3.

Peli1-mediated ubiquitination-dependent degradation of YB-1

As shown in Fig. 3A, ox-LDL treatment reduced the ubiquitination level of YB-1 in Raw264.7 cells. As revealed by CHX chase assay, ox-LDL treatment facilitated YB-1 protein stability (Fig. 3B). To determine the cell specificity of YB-1 degradation, MOVAS and Bend.3 cells were treated with ox-LDL followed by CHX treatment to assess YB-1 protein stability. As shown in Supplementary Fig. 3, ox-LDL treatment did not affect the degradation rate of YB-1 in MOVAS cells (Supplementary Fig. 3A). Conversely, in Bend.3 cells, ox-LDL treatment significantly reduced the degradation rate of YB-1 (Supplementary Fig. 3B), suggesting a regulatory effect of ox-LDL on YB-1 protein stability in endothelial cells. These results indicated that the degradation of YB-1 exhibited cell differences. We reviewed the literature and obtained 14 ubiquitination enzymes that function in AS (Supplementary Table 2). Among them, Peli1, WWP2, SYVN1, March1, and MKRN1, these 5 E3 ubiquitination ligases, were reported to be downregulated in AS[15,21–24]. As shown in Supplementary Fig. 4A, B, bioinformatics prediction results showed that SYVN1 and Peli1 were potential ubiquitinases targeting YB-1. We subsequently conducted IP experiments using YB-1 antibody and detected the levels of Peli1 and SYVN1 E3 ubiquitinase in IP products, and the result showed that only Peli1 showed significant enrichment (Supplementary Fig. 4C, Fig. 3C). As shown in Supplementary Fig. 5A, Peli1-pcDNA3.1 transfection resulted in increased Peli1 protein level in Raw264.7 cells, suggesting the transfection was successful. We then constructed a Peli1 overexpression vector with 6X His tag (His-Peli1-pcDNA3.1) and a YB-1 overexpression vector with HA tag (HA-YB-1-pcDNA3.1) and transfected them simultaneously into 293T cells. We used IgG, 6X His, and HA antibodies for IP, and Western blot was used to detect the levels of 6X His and HA proteins in the IP products. The results showed that YB-1 was enriched in the IP products of His antibody, and Peli1 was enriched in the IP products of HA antibody (Fig. 3D). In addition, it was observed that Peli1

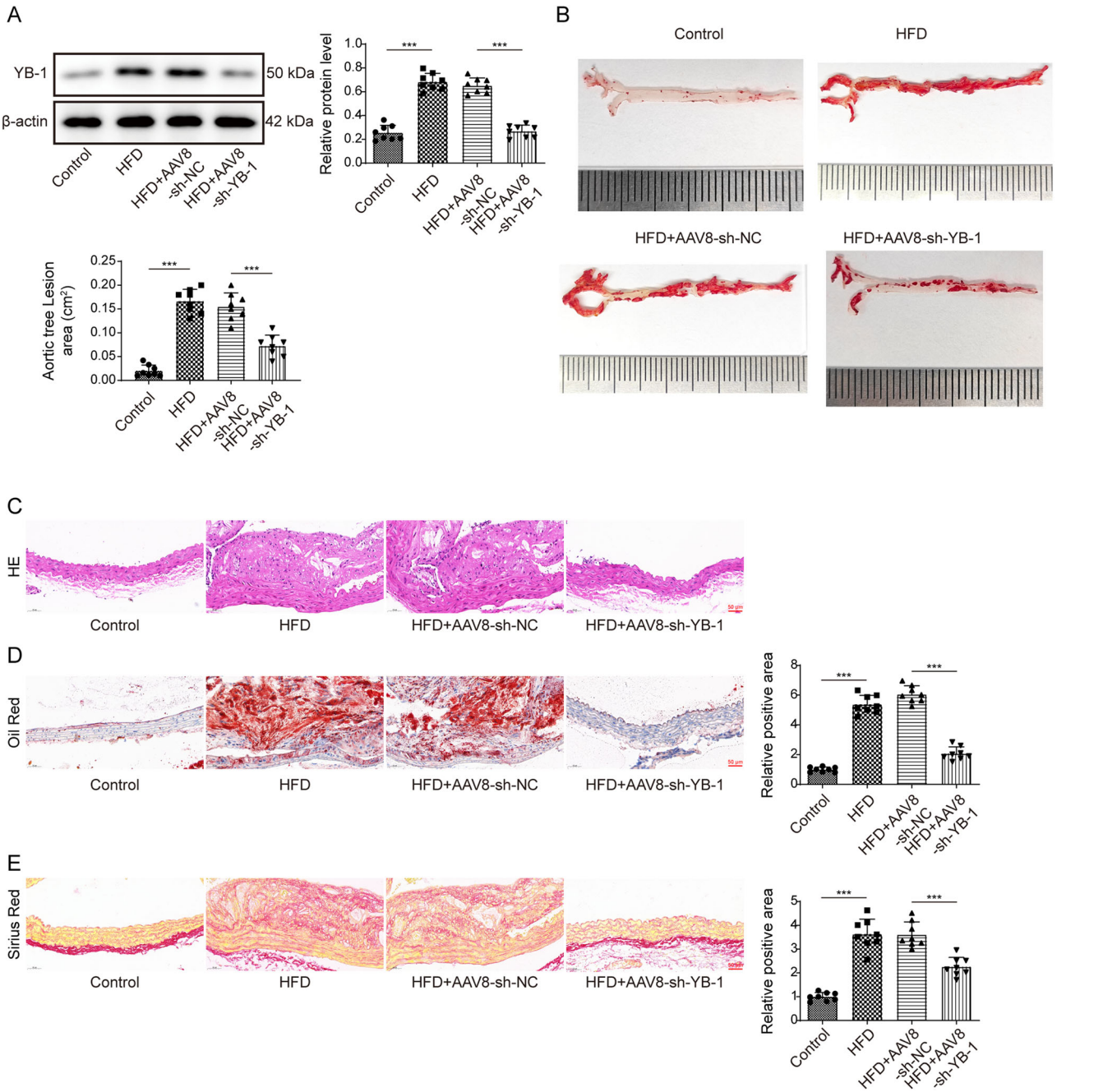

Fig. 1 | YB-1 knockdown inhibited AS progression in vivo. YB-1 knockdown was induced in *ApoE*$^{-/-}$ mice combined with HFD treatment. **A** YB-1 protein level in arterial tissues was examined by western blot. **B** The atherosclerotic lesions of whole artery were observed using Oil Red O staining, and the atherosclerotic lesions of whole artery were quantified. **C** HE staining was adopted to analyze lesions in arterial tissues. **D**, **E** Lipid accumulation in arterial tissues was measured by Oil red O staining and Sirius red staining. Scale bars represent 50 μm. $n = 8$ animals. The measurement data were presented as mean ± SD. Comparisons between two groups were performed using the Student's *t*-test, while multiple group comparisons were made using one-way ANOVA. ***$p < 0.001$. AS atherosclerosis, YB-1 Y-box binding protein 1, ApoE$^{-/-}$ apolipoprotein E-deficient, HFD high-fat diet, HE hematoxylin-eosin, SD standard deviation, ANOVA one-way analysis of variance.

Table 1 | The plasma TC, TG, HDLC, and LDLC levels in different groups of mice

	Control	HFD	HFD + AAV8-sh-NC	HFD + AAV8-sh-YB-1
TC (mM)	6.18 ± 0.71	15.03 ± 0.91	15.68 ± 0.62	8.61 ± 0.87
TG (mmol/g prot)	1.09 ± 0.22	3.94 ± 0.34	4.51 ± 0.39	1.68 ± 0.43
HDLC (mM)	1.13 ± 0.19	1.67 ± 0.14	1.77 ± 0.11	2.67 ± 0.22
LDLC (mM)	6.51 ± 0.53	12.55 ± 0.53	12.07 ± 0.58	8.7 ± 0.38

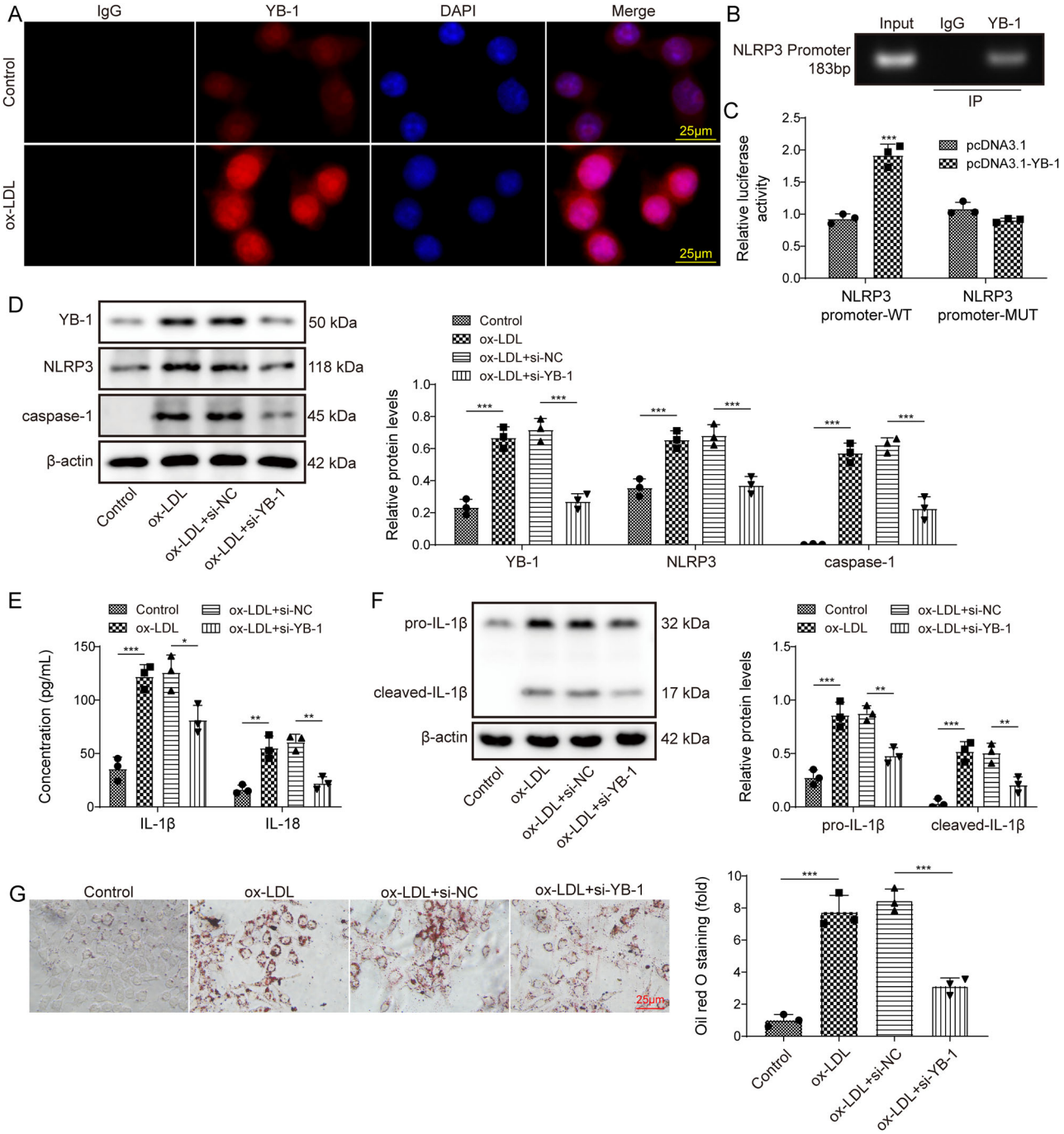

Fig. 2 | YB-1 promoted ox-LDL-induced lipid accumulation in macrophages by regulating NLRP3. A Raw264.7 cells stimulated by ox-LDL were used as AS cellular model, and immunofluorescence was performed to detect nuclear localization in cells. Scale bars represent 25 μm. **B**, **C** ChIP and dual-luciferase reporter gene assays were employed to analyze the interaction between YB-1 and NLRP3 promoter. YB-1 knockdown was induced in ox-LDL-treated Raw264.7 cells. **D** Western blot was adopted to determine YB-1, NLRP3 and caspase-1 levels. **E** IL-1β and IL-18 levels were analyzed using ELISA. **F** The protein levels of cleaved IL-1β and pro-IL-1β in cells were examined by western blot. **G** Lipid accumulation was measured by Oil red O staining. Scale bars represent 25 μm. $n = 3$ independent experiments. The measurement data were presented as mean ± SD. Comparisons between two groups were performed using the Student's *t-test*, while multiple group comparisons were made using one-way ANOVA. $^{*}p < 0.05$, $^{**}p < 0.01$, $^{***}p < 0.001$. ox-LDL oxidized low-density lipoprotein, AS atherosclerosis, ChIP chromatin immunoprecipitation, YB-1 Y-box binding protein 1, NLRP3 nucleotide-binding domain (NOD)-like receptor (NLR) family pyrin domain-containing protein 3, IL Interleukin, ELISA enzyme-linked immunosorbent assay, SD standard deviation, ANOVA one-way analysis of variance.

overexpression reduced YB-1 level in Raw264.7 cells, while this effect was abrogated by MG132 (Proteasome inhibitor) treatment (Fig. 3E). Moreover, Peli1 overexpression reduced YB-1 protein stability in ox-LDL-treated Raw264.7 cells (Fig. 3F). Taken together, Peli1-mediated ubiquitination-dependent degradation of YB-1 during AS progression.

Peli1 was regulated by m^{6}A modification

It was revealed by m^{6}A dot blot assay, ox-LDL treatment increased total m^{6}A level in Raw264.7 cells (Fig. 4A). It was also turned out that the m^{6}A modification level of Peli1 in Raw264.7 cells was markedly increased by ox-LDL stimulation (Fig. 4B). Meanwhile, the m^{6}A modification level of Peli1

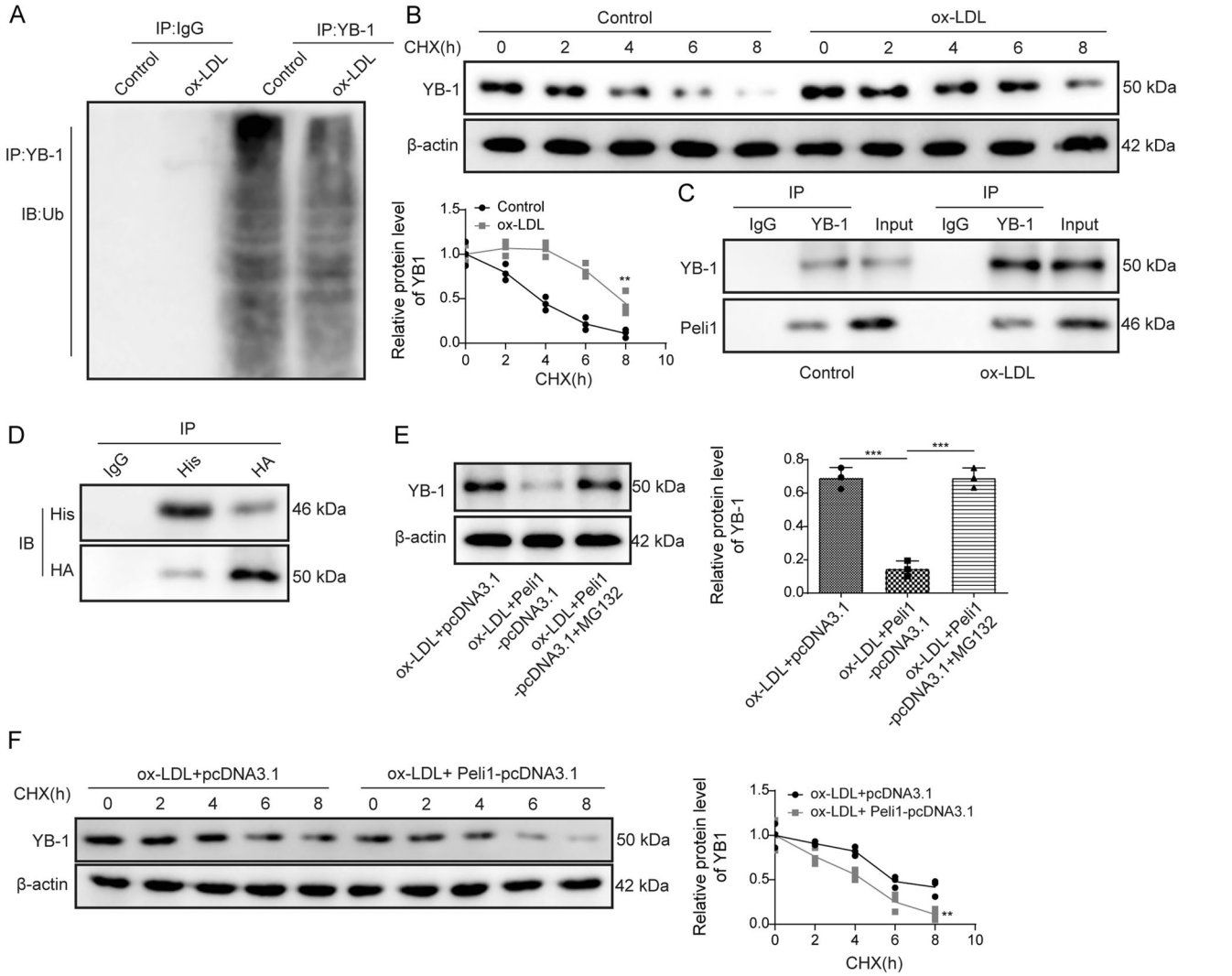

Fig. 3 | Peli1-mediated ubiquitination-dependent degradation of YB-1. A YB-1 ubiquitination level in Raw264.7 cells after ox-LDL treatment was assessed using western blot, and IgG served as the negative control. **B** CHX chase assay was performed to analyze the protein stability of YB-1 in Raw264.7 cells after ox-LDL treatment. **C** The interaction between YB-1 and Peli1 was analyzed using CoIP assay. **D** IP was employed to detect the interaction between YB-1 and Peli1 using a Peli1 overexpression vector with 6X His tag (His-Peli1-pcDNA3.1) and a YB-1 overexpression vector with HA tag (HA-YB-1-pcDNA3.1). **E** Peli1 overexpression was induced in ox-LDL treated Raw264.7 cells combined with MG132 treatment, and YB-1 protein level in cells was examined using western blot. **F** CHX chase assay was performed to analyze the protein stability of YB-1 in ox-LDL-treated Raw264.7 cells after Peli1-pcDNA3.1 or pcDNA3.1 transfection. $n = 3$ independent experiments. The measurement data were presented as mean ± SD. Comparisons between two groups were performed using the Student's t-test, while multiple group comparisons were made using one-way ANOVA. $^{**}p < 0.01$, $^{***}p < 0.001$. YB-1 Y-box binding protein 1, ox-LDL oxidized low-density lipoprotein, CHX cycloheximide, Co-IP coimmunoprecipitation, IP immunoprecipitation, SD standard deviation, ANOVA one-way analysis of variance.

in arterial tissues of *ApoE*$^{-/-}$ mice was significantly increased by HFD (Fig. 4C). METTL3, as a m^{6}A writer, functions in catalyzing the formation of m^{6}A[25]. As demonstrated by RNA pull-down assay, METTL3 directly bound with Peli1 (Fig. 4D). In addition, METTL3 knockdown (Supplementary Fig. 5B) reduced the m^{6}A modification level of Peli1 in Raw264.7 cells (Fig. 4E). Moreover, METTL3 knockdown increased Peli1 expression level in Raw264.7 cells (Fig. 4F, G). In summary, METTL3 negatively regulated Peli1 expression level by increasing the m^{6}A modification level of Peli1 during AS progression.

YTHDC2 recognized m^{6}A modified Peli1 and mediated its mRNA degradation

YTHDC2, a m^{6}A reader, is involved in regulating RNA degradation by recognizing RNA m^{6}A modification[26]. It was revealed that YTHDC2 bound with Peli1 mRNA (Fig. 5A, B). In addition, YTHDC2 overexpression (Supplementary Fig. 5C) reduced Peli1 expression level in ox-LDL-treated Raw264.7 cells, while this effect was reversed by METTL3 knockdown (Fig. 5C, D). It was revealed by RNA degradation assay that Peli1 mRNA stability in ox-LDL-treated Raw264.7 cells was reduced by YTHDC2 overexpression, which was abrogated after si-METTL3 transfection (Fig. 5E). In conclusion, YTHDC2 recognized METTL3-mediated Peli1 m^{6}A modification and mediated Peli1 mRNA degradation.

Peli1 inhibited the activation of NLRP3 inflammasome in macrophages through ubiquitination of YB-1

To investigate the regulatory relationship between Peli1 and YB-1 in AS, Raw264.7 cells were co-transfected with YB-1-pcDNA3.1 and Peli1-pcDNA3.1 and subsequently subjected to ox-LDL. As shown in Fig. 6A, Peli1 overexpression ameliorated ox-LDL-induced increase in YB-1, NLRP3 and caspase-1 levels in Raw264.7 cells, while these effects were reversed by YB-1 overexpression. The results of Enzyme-linked immunosorbent assay (ELISA) subsequently revealed that ox-LDL-mediated IL-1β and IL-18 upregulation in Raw264.7 cells was ameliorated following Peli1 overexpression, which was abrogated by YB-1 overexpression (Fig. 6B). As

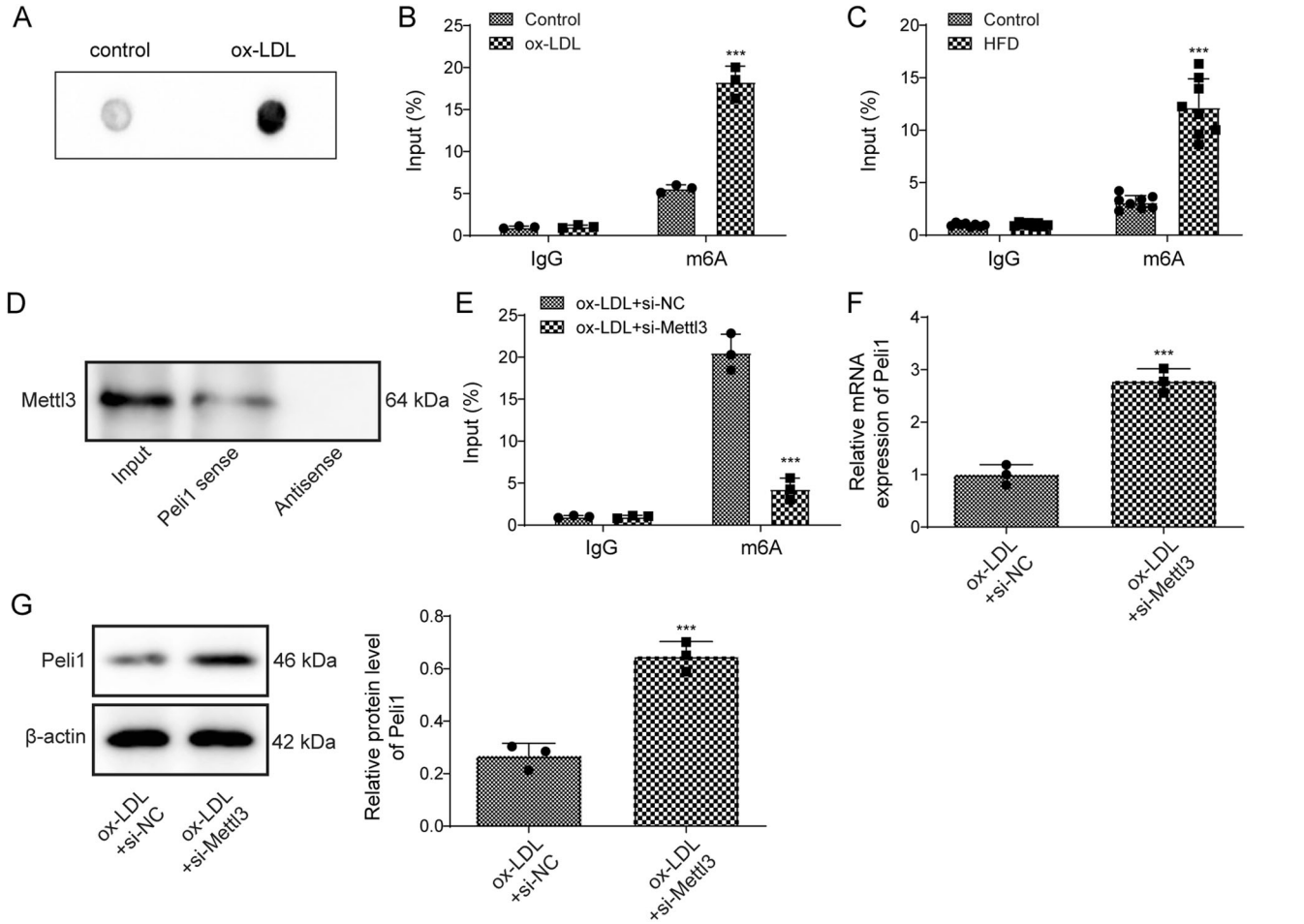

Fig. 4 | Peli1 was regulated by m^{6}A modification. A m^{6}A dot blot assay was conducted to analyze total m^{6}A level in Raw264.7 cells after ox-LDL treatment. **B** The m^{6}A level of Peli1 in Raw264.7 cells after ox-LDL treatment was examined using MeRIP assay. **C** The m^{6}A level of Peli1 in arterial tissues was examined using MeRIP assay. **D** The interaction between METTL3 and Peli1 was analyzed using RNA pull-down assay. **E** The m^{6}A level of Peli1 in ox-LDL treated Raw264.7 cells after METTL3 knockdown was examined using MeRIP assay. **F**, **G** Peli1 expression level in ox-LDL treated Raw264.7 cells after METTL3 knockdown was examined using qRT-PCR and western blot. $n = 3$ independent experiments. The measurement data were presented as mean ± SD. Comparisons between two groups were performed using the Student's t-test. ***$p < 0.001$. m^{6}A N6-methyladenosine, Peli1 pellino 1, MeRIP methylated RNA immunoprecipitation, METTL3 methyltransferase-like 3, ox-LDL oxidized low-density lipoprotein, qRT-PCR quantitative real-time polymerase chain reaction, SD standard deviation.

shown in Fig. 6C, Peli1 overexpression reduced the protein levels of cleaved IL-1β and pro-IL-1β in ox-LDL-treated Raw264.7 cells, while these effects were reversed by YB-1 overexpression. It also turned out that Peli1 overexpression inhibited ox-LDL-mediated lipid accumulation in macrophages, which was reversed by YB-1 overexpression (Fig. 6D). As reported, the knockdown of Peli1 produced anti-inflammatory and anti-apoptotic effects by targeting the TLR signaling pathway in chondrocytes[27]. Our results showed that Peli1 overexpression did not significantly affect Traf3 protein level in ox-LDL-treated Raw264.7 cells (Supplementary Fig. 6), indicating Peli1-mediated IL-1β regulation was independent of the TLR pathway. Collectively, Peli1 inhibited the activation of NLRP3 inflammasome in macrophages to suppress ox-LDL-induced lipid accumulation through ubiquitination of YB-1.

Peli1 inhibited AS progression in vivo through ubiquitination of YB-1

To further investigate the regulatory relationship between Peli1 and YB-1 in AS, Peli1 overexpression and YB-1 overexpression were induced in *ApoE*$^{-/-}$ mice combined with HFD treatment. It was firstly observed that Peli1 overexpression ameliorated HFD-induced increase in YB-1, NLRP3 and caspase-1 levels in arterial tissues, while these effects of Peli1 overexpression were abrogated by YB-1 overexpression (Fig. 7A). It was also observed that Peli1 overexpression increased the ubiquitination level of YB-1 in arterial tissues of *ApoE*-/- mice (Fig. 7B). Plasma TC, TG, HDLC and LDLC levels were subsequently detected, and the results revealed that Peli1 upregulation decreased plasma TC, TG and LDLC levels and increased HDLC level in HFD-treated *ApoE*-/- mice, while YB-1 overexpression reversed the above changes (Table 2). It turned out that Peli1 overexpression mitigated HFD-induced increase in lipid accumulation in the whole artery, while this effect of Peil1 overexpression was partially reversed by YB-1 overexpression (Fig. 7C). In addition, it was observed that HFD-induced lesions and lipid accumulation in arterial tissues were ameliorated by Peli1 overexpression, which was reversed by YB-1 overexpression (Fig. 7D–F). Furthermore, HFD-mediated serum IL-1β and IL-18 upregulation was ameliorated by Peli1 overexpression, which was abolished by YB-1 overexpression (Fig. 7G). Collectively, YB-1 upregulation abrogated Peli1 overexpression's repression on AS development in vivo.

Discussion

AS is a common cardiovascular disease and a significant risk factor for coronary heart disease and cerebral infarction, which lacks effective treatment strategies[28]. The NLRP3 inflammasome activates caspase-1, secretes pro-IL-1β and pro-IL-18 under pathological conditions of inflammation[29]. Notably, NLRP3 inflammasome is activated in AS by crystalline cholesterol

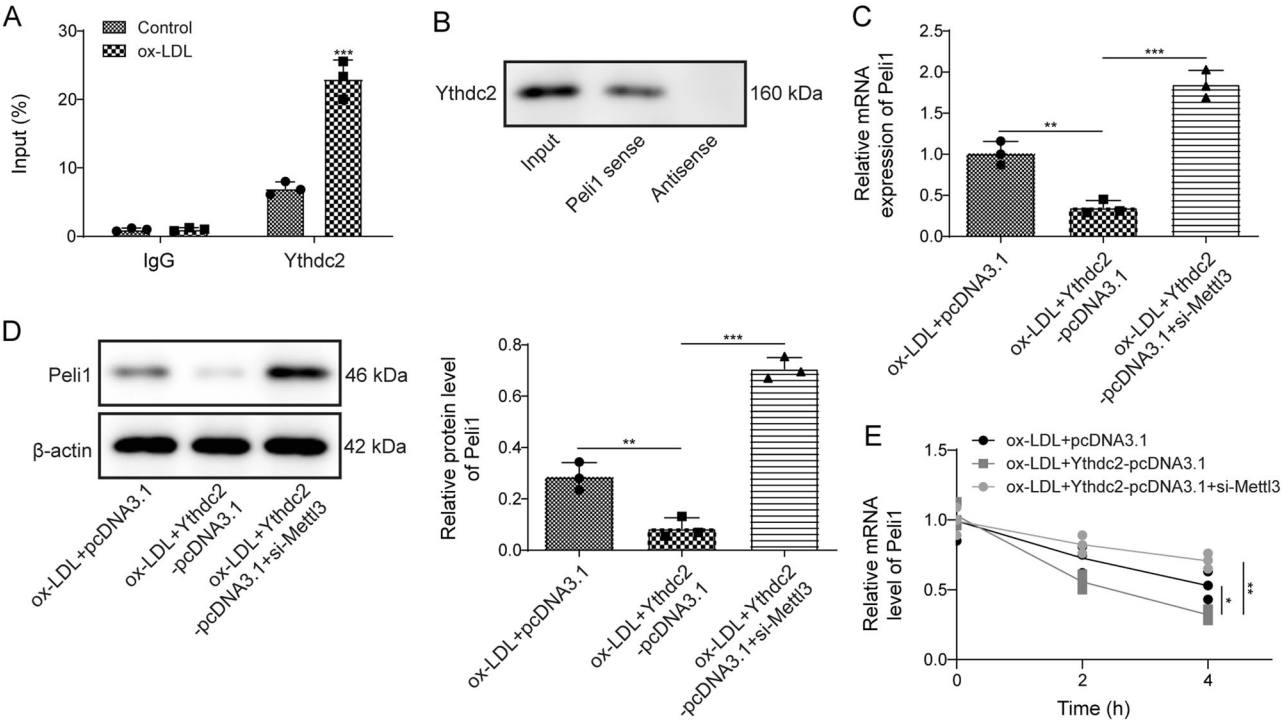

Fig. 5 | YTHDC2 recognized m^{6}A modified Peli1 and mediated its mRNA degradation. A, **B** The interaction between YTHDC2 and Peli1 was analyzed using RIP and RNA pull-down assays. **C**, **D** YTHDC2 overexpression and METTL3 knockdown were induced in ox-LDL-treated Raw264.7 cells. **C**, **D** Peli1 expression level was measured by qRT-PCR and western blot. **E** RNA degradation assay was employed to analyze Peli1 mRNA stability in cells. $n = 3$ independent experiments. The measurement data were presented as mean ± SD. Comparisons between two groups were performed using the Student's t-test, while multiple group comparisons were made using one-way ANOVA. $^*p < 0.05$, $^{**}p < 0.01$, $^{***}p < 0.001$. YTHDC2 YTH domain-containing protein 2, Peli1 pellino 1, RIP RNA immunoprecipitation, METTL3 methyltransferase-like 3, ox-LDL oxidized low-density lipoprotein, SD standard deviation, ANOVA one-way analysis of variance.

and ox-LDL[30]. The activation of NLRP3 inflammasome in macrophages is recognized as a crucial AS event[30]. Inhibiting the activation of NLRP3 inflammasome in macrophages might be a potential therapeutic strategy for AS. The primary findings in the current research are that Peli1, regulated by m^{6}A modification, inhibits YB-1-mediated activation of NLRP3 inflammasome in macrophages by promoting YB-1 ubiquitination to repress AS progression.

Transcription factor YB-1, as a mediator of inflammatory processes, is involved in AS progression through the transcriptional control of inflammation-related genes[31]. Ewert et al. revealed that YB-1 knockdown significantly decreased the number of lesional macrophages in AS mice[32]. In addition, YB-1 knockdown could inhibit AS progression by repressing abnormal proliferation of VSMCs[11]. Consistently, our results revealed that YB-1 knockdown ameliorated lesions and lipid accumulation in arterial tissues of AS mice. Notably, it was previously reported that YB-1 inhibition contributed to NLRP3 inflammasome inactivation in acute liver failure[12]. Herein, it was found that YB-1 transcriptionally activated NLRP3 expression. As expected, YB-1 knockdown inhibited ox-LDL-mediated lipid accumulation and inflammation in macrophages by inactivating NLRP3 inflammasome. All our results suggested that YB-1 could contribute to lipid accumulation and inflammatory factor secretion in macrophages to aggravate AS progression by activating NLRP3 inflammasome.

Ubiquitination is an essential post-translational modification that has been well demonstrated to be involved in the pathophysiology of AS[33]. Ubiquitination modification is regulated by ubiquitin-conjugating enzymes, ubiquitin ligases and deubiquitinating enzymes[34]. Peli1, as a ubiquitin ligase, plays a key role in the pathogenesis of inflammatory diseases, including AS[15]. Burger et al. demonstrated that Peli1 deficiency accelerated AS progression by promoting VSMCs foam cells formation[15], revealing the protective role of Peli1 in AS. Herein, we identified YB-1 as the functional target of Peli1 in regulating AS progression. Specifically, Peli1-mediated ubiquitination-dependent degradation of YB-1 in AS. Additionally, as expected, Peli1 overexpression inhibited ox-LDL-mediated lipid accumulation, inflammation and activation of NLRP3 inflammasome in Raw264.7 cells as well as lesions and lipid accumulation in arterial tissues of AS mice, while these effects were all reversed by YB-1 overexpression. Collectively, Peli1 inhibited the activation of NLRP3 inflammasome in macrophages through ubiquitination of YB-1 to repress AS development. A previous study showed that Peli1 could promote the activation of NLRP3 inflammasome[35], which is different from our results, possibly due to the different molecular regulatory mechanisms within cells under different pathological conditions.

As widely described, m^{6}A dysregulation contributes to AS pathogenesis[36]. In the current study, it was found that total m^{6}A level and the m^{6}A level of Peli1 in Raw264.7 cells significantly increased by ox-LDL treatment, indicating that the abnormal expression of Peli1 in AS may be related to its m^{6}A modification dysregulation. METTL3, an m^{6}A writer, functions in regulating various biological processes and disease progression by increasing the m^{6}A modification of downstream targets[37]. As previously described, METTL3 was significantly upregulated in ox-LDL-treated HUVECs, and its knockdown inhibited AS progression in vivo[19]. Herein, our results revealed that METTL3 inhibited Peli1 expression in ox-LDL-treated Raw264.7 cells by increasing the m^{6}A modification level of Peli1. Notably, m^{6}A reader can recognize m^{6}A writer-mediated m^{6}A modification to regulate the stability and translation of downstream targets. For example, YTHDC2 recognized METTL3-mediated m^{6}A modification of Lrp2 to promote neurogenesis[38]. Herein, it was found that YTHDC2 directly bound with Peli1 mRNA. Moreover, YTHDC2 overexpression markedly reduced Peli1 mRNA stability and expression in ox-LDL-treated Raw264.7 cells, which was abolished by METTL3 knockdown, Therefore, we came the conclusion that YTHDC2 recognized METTL3-mediated Peli1 m^{6}A modification and mediated Peli1 mRNA degradation. Plaque stability and the phenotypic switch of vascular smooth muscle cells (VSMCs) are critical

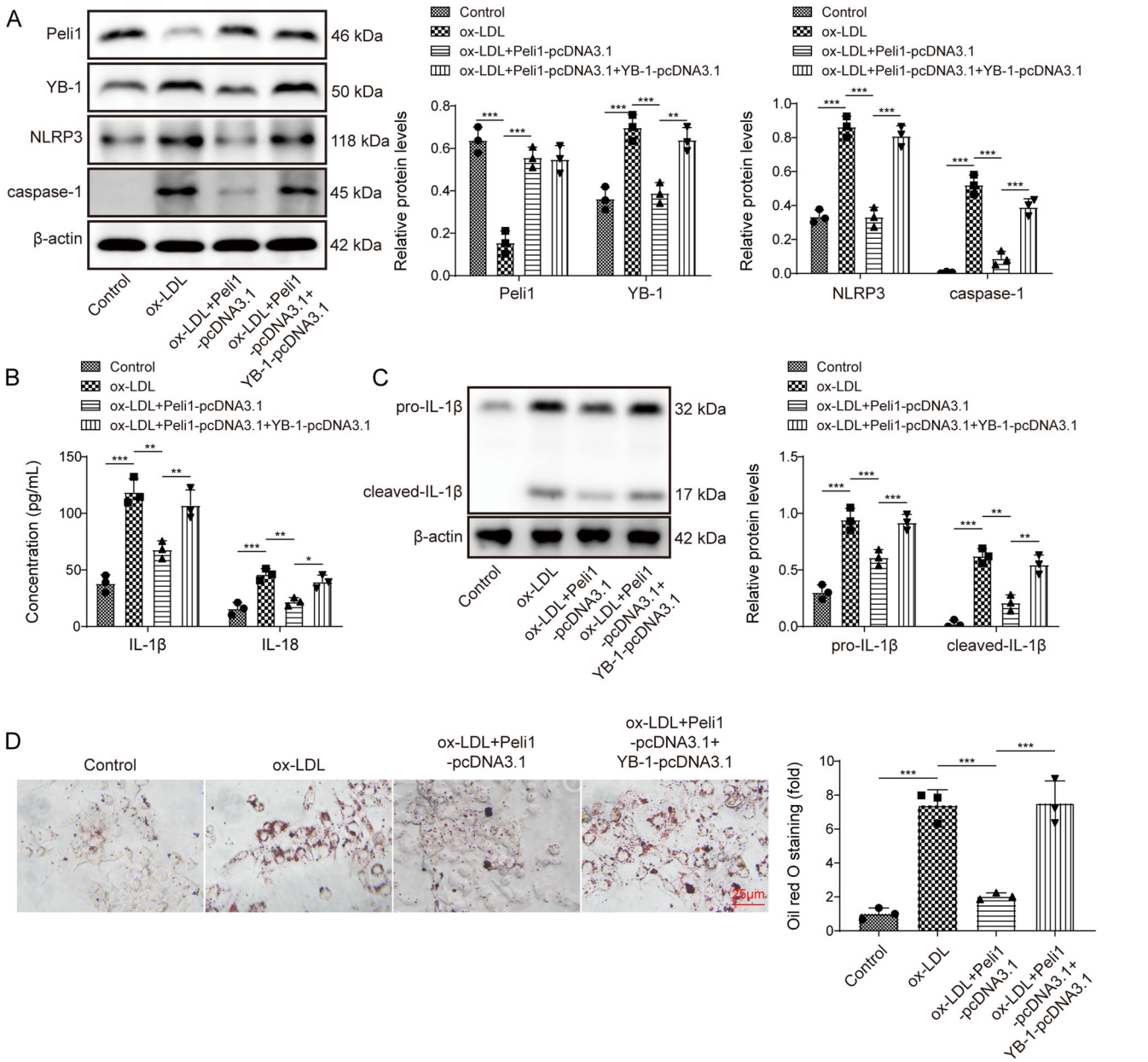

Fig. 6 | Peli1 inhibited the activation of NLRP3 inflammasome in macrophages through ubiquitination of YB-1. Peli1 overexpression and YB-1 overexpression were induced in Raw264.7 cells and ox-LDL treatment was subsequently performed. **A** YB-1, NLRP3 and caspase-1 levels were measured using western blot. **B** IL-1β and IL-18 levels were analyzed using ELISA. **C** The protein levels of cleaved IL-1β and pro-IL-1β in cells were detected by western blot. **D** Lipid accumulation was measured by Oil red O staining. Scale bars represent 25 μm. $n = 3$ independent experiments. The measurement data were presented as mean ± SD. Comparisons between two groups were performed using the Student's *t*-test, while multiple group comparisons were made using one-way ANOVA. $^{*}p < 0.05$, $^{**}p < 0.01$, $^{***}p < 0.001$. Peli1 pellino 1, YB-1 Y-box binding protein 1, ox-LDL oxidized low-density lipoprotein, NLRP3 nucleotide-binding domain (NOD)-like receptor (NLR) family pyrin domain-containing protein 3, IL interleukin, ELISA enzyme-linked immunosorbent assay, SD standard deviation, ANOVA one-way analysis of variance.

in AS[39,40]. VSMCs undergo a phenotypic switch from a contractile to a synthetic state, enabling matrix production and migration to stabilize plaques[41]. Notably, additional experiments with smooth muscle cells (MOVAS) and endothelial cells (Bend.3) revealed that YB-1 degradation in response to ox-LDL is specific to endothelial cells and macrophages, but not smooth muscle cells. These observations suggested that the degradation of YB-1 exhibits cell differences in AS. However, the role of Peli1/YB-1/NLRP3 in regulating plaque stability and VSMCs phenotypic switch during AS progression is not well known, which is the limitation of this study and needs further in vivo experiments to elucidate it. In addition, the role of Peli1/YB-1/NLRP3 in AS was only studied in macrophages, not in other types of cells. In the future, we will explore this pathway in depth in other cell types to fully elucidate the underlying mechanism and the physiological relevance of the proposed findings in vivo.

Collectively, our research reported that Peli1, regulated by m^6A modification, inhibited YB-1-mediated activation of NLRP3 inflammasome in macrophages by promoting YB-1 ubiquitination to suppress AS progression. These findings systematically elucidate the mechanism of Peli1 in the progression of AS and suggest that targeting Peli1 may be a potential therapeutic approach for AS. While the study provides valuable insights into the role of YB-1 and Peli1 in AS, several limitations should be considered. First, potential sources of bias, despite randomization and blinding, may still arise from factors such as variability in the animal model and technical limitations of experimental procedures. Second, the animal model used,

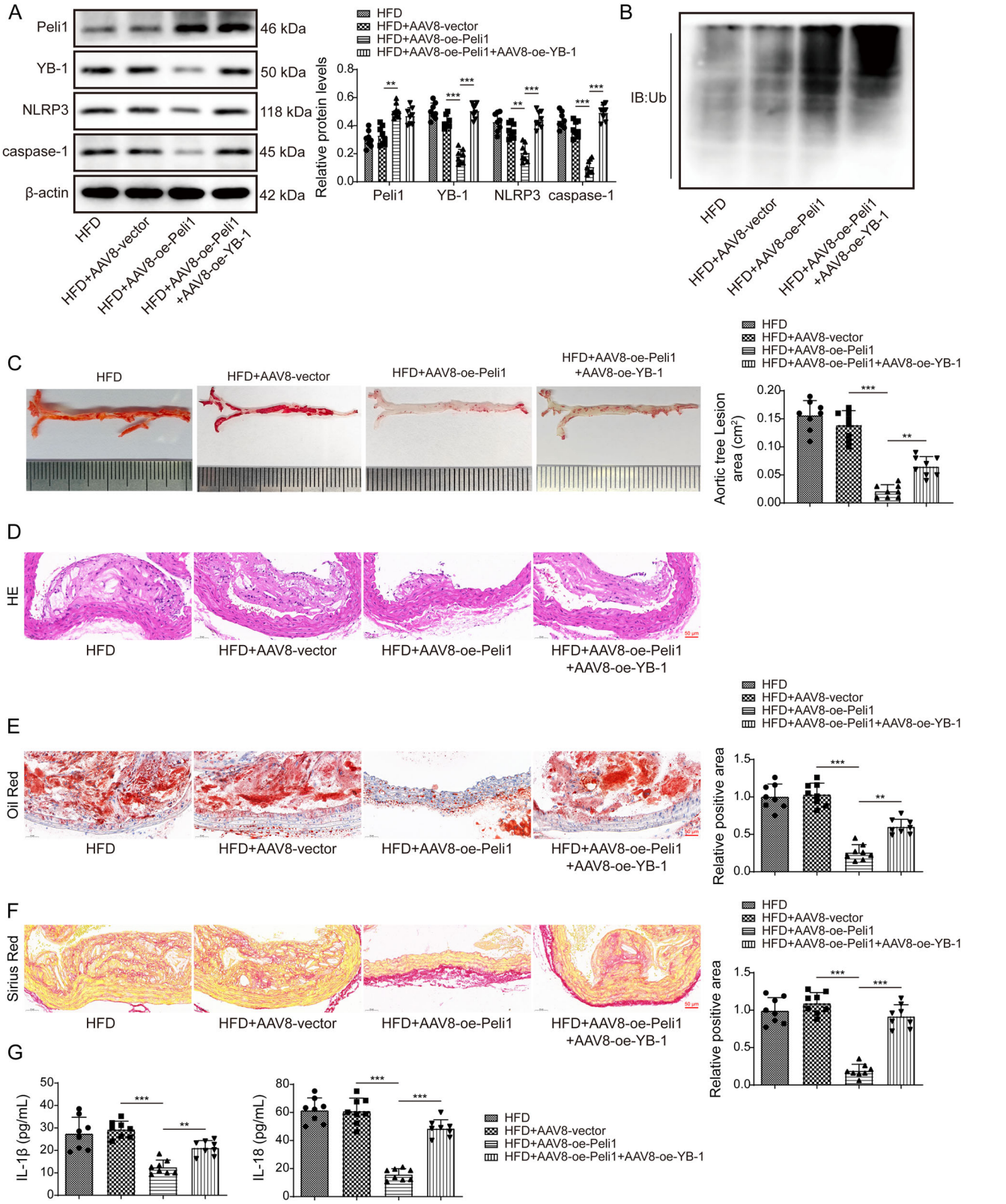

Fig. 7 | Peli1 inhibited AS progression in vivo through ubiquitination of YB-1. Peli1 overexpression and YB-1 overexpression were induced in *ApoE*$^{-/-}$ mice combined with HFD treatment. **A** YB-1, NLRP3 and caspase-1 protein levels in arterial tissues were measured using western blot. **B** Ubiquitination assay was performed to detect ubiquitination level of YB-1 in arterial tissues. **C** The atherosclerotic lesions of whole artery were observed using Oil Red O staining, and the atherosclerotic lesions of whole artery were quantified. **D** HE staining was employed to analyze lesions in arterial tissues. Scale bars represent 50 μm. **E**, **F** Lipid accumulation in arterial tissues was measured by Oil red O staining and Sirius red staining. Scale bars represent 50 μm. **G** Serum IL-1β and IL-18 levels were analyzed using ELISA. $n = 8$ animals. The measurement data were presented as mean ± SD. Comparisons between two groups were performed using the Student's *t*-test, while multiple group comparisons were made using one-way ANOVA. $^{*}p < 0.05$, $^{**}p < 0.01$, $^{***}p < 0.001$. Peli1 pellino 1, YB-1 Y-box binding protein 1, ApoE$^{-/-}$ apolipoprotein E-deficient, HFD high-fat diet, HE hematoxylin-eosin, IL interleukin, ELISA enzyme-linked immunosorbent assay, SD standard deviation, ANOVA one-way analysis of variance.

Table 2 | The plasma TC, TG, HDLC, and LDLC levels in different groups of mice

	HFD	HFD + AAV8-vector	HFD + AAV8-oe-Peli1	HFD + AAV8-oe-Peli1 + AAV8-oe-YB-1
TC (mM)	15.64 ± 0.87	14.59 ± 0.60	6.94 ± 1.05	12.38 ± 0.7
TG (mmol/g prot)	3.76 ± 0.48	3.78 ± 0.38	1.76 ± 0.26	3.36 ± 0.39
HDLC (mM)	1.99 ± 0.31	2.07 ± 0.27	2.64 ± 0.13	2.06 ± 0.29
LDLC (mM)	13.08 ± 0.8	13.69 ± 0.0.66	7.42 ± 0.9	12.81 ± 0.65

ApoE$^{-/-}$ mice, is a well-established model for studying atherosclerosis, but it has limitations. These mice do not fully recapitulate all aspects of human atherosclerosis, particularly with regard to the development of advanced plaque rupture or thrombosis, which are key events in human cardiovascular disease. The findings in this model may not fully reflect the complexity of atherosclerosis in humans, and the response to treatments may differ between species. Future studies using additional models of atherosclerosis, such as those involving genetic modifications that more closely resemble human conditions, could help address this gap.

Methods

Animal experiments

ApoE$^{-/-}$ mice have an impaired ability to clear lipoproteins and easily form extensive atherosclerotic plaque in the blood vessel. In this study, 80 *ApoE*$^{-/-}$ mice (male, 8 weeks old, 20–22 g) were obtained from SJA LABORATORY Animal Co, Ltd. (Hunan, China). The animals were housed in a controlled environment with a 12-h light/dark cycle at 22–24 °C, with relative humidity maintained at 40–60%. The cages were provided with soft bedding (e.g., wood chips) to ensure comfort, and animals had access to food and water ad libitum. The mice were housed in groups of 3–4 per cage to allow for social interaction, which serves as environmental enrichment. To investigate the function of YB-1 in AS, mice were divided into four groups ($n = 8$): control group, HFD group, HFD + AAV8-sh-NC group, and HFD + AAV8-sh-YB-1 group. The sequences of sh-YB-1 and sh-NC are listed in Supplementary Table 3. Meanwhile, to investigate whether Peli1 alleviated AS by regulating YB-1, mice were divided into the following four groups ($n = 8$): HFD group, HFD + AAV8-vector group, HFD + AAV8-oe-Peli1 group, and HFD + AAV8-oe-Peli1 + AAV8-oe-YB-1 group. In addition, to investigate the effect of YB-1 knockdown in macrophages on the progression of AS, mice were divided into the following two groups ($n = 8$): HFD + AAV LysM sh NC group and HFD + AAV-LysM-sh-YB-1 group. AAV8-sh-NC, AAV8-sh-YB-1, AAV8-vector, AAV8-oe-YB-1, AAV8-oe-Peli1, AAV-LysM-sh-NC, and AAV-LysM-sh-YB-1 viruses were constructed by GenePharma (Shanghai, China). The experimental units (mice) were randomly assigned, and the randomization sequence was generated using a computer-based random number generator to ensure unbiased allocation of mice to different experimental groups. The tail veins of the HFD + AAV8-sh-NC, HFD + AAV8-sh-YB-1, HFD + AAV8-vector, HFD + AAV8-oe-Peli1, HFD + AAV8-oe-Peli1 + AAV8-oe-YB-1, AAV-LysM-sh-NC, and AAV-LysM-sh-YB-1 groups were injected with 200 μL of the corresponding AAVs at a titer of 1×10^9 eg/mL. To minimize potential confounders, the order of treatments was randomized for each animal, and cage positions were rotated within the animal facility to reduce location-based environmental factors such as light, temperature, or humidity that could influence the outcomes. After 2 weeks, the HFD groups (*ApoE*$^{-/-}$ mice) were fed with HFD containing 40% fat, 1.25% cholesterol, and 0.5% cholic acid. To minimize pain, suffering, and distress, appropriate interventions were implemented. The mice were monitored throughout the study for signs of distress, such as changes in behavior, fur condition, posture, and activity level. When administering treatments, including injections or surgeries, anesthesia was used to prevent pain. Anesthesia was induced using isoflurane (2–3% in oxygen), and analgesics were provided post-surgery or post-treatment to minimize discomfort. If any animal showed signs of excessive distress or weight loss greater than 20% of its body weight, it was removed from the study and provided with appropriate veterinary care. The mice were euthanized after 12 weeks, and arterial tissues and plasma were collected. We have complied with all relevant ethical regulations for animal use. The animal studies were approved by the ethics committee of the Second Affiliated Hospital of Nanchang University (Review [2023] No. (323)).

Measurement of plasma TC, TG, HDLC and LDLC levels

Plasma TC, TG, HDLC and LDLC levels were examined using the TC assay kit (Jiancheng, Nanjing, China, F002-1-1), TG assay kit (Jiancheng, F001-1-1), HDLC assay kit (Jiancheng, A112-1-1) and LDLC assay kit (Jiancheng, A113-1-1) in according to the manuals. Plasma samples were first separated by centrifugation at 3000 rpm for 10 min. For TC measurement, a colorimetric method was employed where the cholesterol in the sample was hydrolyzed and reacted with reagents to form a colored product, with the absorbance measured at 520 nm. For TG, lipase-mediated hydrolysis of triglycerides was followed by a colorimetric reaction, with absorbance measured at 510 nm. HDLC levels were measured after precipitating non-HDL lipoproteins and analyzing the supernatant with a colorimetric assay at 600 nm. LDLC was quantified after precipitation of VLDL and chylomicrons, and the remaining fraction was analyzed using a colorimetric method with absorbance taken at 600 nm. The standard solutions provided in the kits were used to generate a standard curve for quantifying the lipid concentrations.

Hematoxylin-eosin (HE) staining

The arterial tissue blocks were fixed in 4% paraformaldehyde at room temperature for 24 h to preserve cellular and tissue structure. Following fixation, the tissues were dehydrated in a graded series of alcohol concentrations (70%, 80%, 90%, 95%, and 100%) for 1 h at each concentration, followed by clearing in xylene to remove alcohol. After dehydration and clearing, the tissues were embedded in paraffin at 60 °C, and 5 μm thick sections were cut using a rotary microtome. The sections were then mounted onto glass slides and allowed to dry at room temperature. For HE staining, the sections were deparaffinized by incubating them in xylene and rehydrated by passing them through a descending series of alcohol concentrations (100%, 95%, 90%, 80%, and 70%) for 5 min each. The sections were then washed in distilled water before staining. The sections were stained with hematoxylin (Sigma-Aldrich, MO, USA) for 5–10 min, followed by a rinse in running tap water, and then stained with eosin for 2–3 min. After staining, the sections were dehydrated again in the ascending series of alcohol concentrations (70%, 80%, 90%, 95%, and 100%) for 5 min each and cleared in xylene. The stained sections were mounted with a coverslip using neutral resin. Finally, the morphological features of the stained tissue sections were observed and photographed under a light microscope (Nikon, Tokyo, Japan) at appropriate magnifications for the analysis of histological changes in the arterial tissues.

Immunofluorescence of tissues

The arterial tissue sections were first fixed using cold methanol for 40 min at −20 °C to preserve cellular structures and reduce background staining. After fixation, the sections were incubated overnight at 4 °C with primary antibodies against CD68 (1:50, ab955, Abcam, Cambridge, UK) and YB-1 (1:100, ab76149, Abcam) to target macrophages and YB-1, respectively. Following overnight incubation, the sections were washed three times with

PBS to remove any unbound antibodies. The tissue sections were then incubated with the appropriate secondary antibody at 25 °C for 1 h, which facilitated the detection of the primary antibody binding. After secondary antibody incubation, the sections were counterstained with 4′,6-diamidino-2-phenylindole (DAPI) for 5 min to label the nuclei and enhance visualization of the tissue structures. The sections were then mounted with a mounting medium and visualized using a Zeiss LSM 880 confocal microscope (Oberkohen, Germany) equipped with appropriate filters for fluorescence detection.

Oil red O staining and Sirius red staining

The arterial tissue sections were prepared by freezing the tissue blocks at −80 °C for at least 1 h. Once frozen, the tissue was sectioned into 5 μm thick slices using a cryostat (Leica) at −20 °C to maintain tissue integrity. The frozen sections were then mounted onto glass slides and allowed to air dry at room temperature for 30 min to ensure proper attachment to the slides. For Oil Red O staining, the sections were first fixed in 4% paraformaldehyde for 10 min at room temperature to preserve the tissue morphology. After fixation, the sections were washed in PBS and incubated with 0.5% Oil Red O solution (Sigma-Aldrich) in isopropanol for 15 min at room temperature. After incubation, the slides were washed with 60% isopropanol to remove excess stain and then counterstained with hematoxylin for 1 min to visualize the cell nuclei. The stained sections were observed under a Nikon light microscope at 200× magnification, and images were captured to evaluate lipid accumulation in the arterial tissue. For Sirius Red staining, the sections were first hydrated by passing through a series of alcohol solutions (100%, 95%, and 70%) and then washed in distilled water. The tissue sections were incubated with Sirius Red solution (KeyGEN BioTECH, Nanjing, China) for 1 h at room temperature to stain collagen fibers. After staining, the sections were washed in acidified water (0.5% acetic acid) to remove excess dye, followed by dehydration in increasing concentrations of alcohol (70%, 95%, and 100%). Finally, the sections were cleared in xylene and mounted using a mounting medium. The stained sections were examined under a microscope (Nikon) at 200× magnification for collagen deposition and tissue fibrosis.

Cell culture and treatment

Raw264.7, 293T cells, MOVAS (mouse aortic smooth muscle cells), and Bend.3 (mouse vascular endothelial cells), obtained from ATCC (VA, USA), were cultured in DMEM (Gibco, MD, USA) containing 10% FBS (Gibco) at 37 °C with 5% CO_2. To establish in vitro AS model, Raw264.7, MOVAS, and Bend.3 cells were subjected to 50 μg/mL oxidized low-density lipoprotein (ox-LDL, Solarbio, Beijing, China) for 24 h. Cells were subjected to cycloheximide (CHX, 5 μM, 0, 2, 4, 6 and 8 h) and proteasome inhibitor MG132 (5 μM, 12 h).

Cell transfection

The small interfering RNA of YB-1 (si-YB-1), the small interfering RNA of METTL3 (si-METTL3), the overexpression plasmid of YTHDC2 (YTHDC2-pcDNA3.1), the overexpression plasmid of YB-1 (YB-1-pcDNA3.1), the overexpression plasmid of Peli1 (Peli1-pcDNA3.1), the overexpression plasmid of NLRP3 (NLRP3-pcDNA3.1) and their negative controls were transfected into cells with Lipofectamine™ 3000 (Invitrogen, CA, USA). Lipofectamine™ 3000 was mixed with Opti-MEM® I Reduced Serum Medium (Gibco), and the siRNAs and plasmids (typically 50–100 nM for siRNA and 1–2 μg for plasmids per well in 6-well plates) were incubated with the Lipofectamine™ 3000 reagent for 20 min at room temperature to form transfection complexes. These complexes were then added to the cell cultures, and the cells were incubated for 6 h at 37 °C in a 5% CO_2 incubator. After the transfection period, the culture medium was replaced with fresh complete medium, and the cells were incubated for 48 h. The above plasmids were all obtained from GenePharma (Shanghai, China). The sequences of si-METTL3, si-YB-1, and si-NC are listed in Supplementary Table 3.

Oil red O staining of cells

RAW264.7 cells were fixed with 4% paraformaldehyde for 30 min at room temperature to preserve cell morphology. After fixation, the cells were washed three times with PBS to remove any residual paraformaldehyde. To visualize lipid accumulation, cells were then incubated with Oil Red O working solution (Sigma-Aldrich) for 15 min at 60 °C. The Oil Red O solution was freshly prepared by dissolving 0.5% Oil Red O in isopropanol, followed by dilution in PBS (3:2 ratio). After the incubation, cells were washed twice with PBS to remove excess dye, followed by counterstaining with hematoxylin (1 min) to visualize the cell nuclei. The stained cells were observed under a Nikon light microscope at 200× magnification.

Quantitative real-time polymerase chain reaction (qRT-PCR)

TRIzol (ThermoFisher Scientific, MA, USA) was adopted to isolate total RNA. The cDNA was synthesized using the reverse-transcription kit (Toyobo, Tokyo, Japan) and subjected to the qRT-PCR assay with SYBR (ThermoFisher Scientific). *GAPDH* was used as the reference gene. The data was analyzed with the $2^{-\Delta\Delta CT}$ method. The primers were listed as follows (5'-3'):

Peli1 (F): GCCCCAGTAAAATATGGCGAA
Peli1 (R): CCCCATTTGCCTTAGGTCTTT
GAPDH (F): AGGTCGGTGTGAACGGATTTG
GAPDH (R): TGTAGACCATGTAGTTGAGGTCA

ELISA

IL-1β and IL-18 levels were examined using mouse IL-1β ELISA kit (Abcam, Cambridge, UK, ab197742) and mouse IL-18 ELISA kit (Cusabio, TX, USA, CSB-E04609m) according to the manuals. For the assay, cell supernatants were first collected and centrifuged at 1000×*g* for 10 min at 4 °C to remove any particulate matter. The supernatants were then carefully transferred to new tubes. The ELISA assays were performed in 96-well microplates precoated with the capture antibody. The samples were added to the wells in duplicate, followed by the addition of the detection antibody and incubation at room temperature or 4 °C for 1 h. After washing the wells to remove unbound material, a substrate solution was added to the wells. The reaction was developed, and the absorbance was measured at 450 nm using a microplate reader (BioTek, CA, USA). Concentrations of IL-1β and IL-18 were determined by comparing the absorbance values to a standard curve generated using known concentrations of recombinant IL-1β and IL-18 provided in the respective kits. The results were expressed in picograms per milliliter (pg/mL), and data were analyzed using GraphPad Prism software (version X). The detection limits of the assays, as specified by the manufacturer, were also reported.

Western blot

The proteins were isolated with RIPA, and the protein concentration was analyzed using BCA kit (Beyotime). Then the same amount of protein was separated by 12% PAGE gel, which further transferred to a PVDF membrane (Millipore, MA, USA), and the membranes were blocked and incubated with antibodies against METTL3 (Abcam, 1:1000, ab195352), YTHDC2 (Abcam, 1:1000, ab220160), Peli1 (Abcam, 1:1000, ab199336), YB-1 (Abcam, 1:1000, ab76149), NLRP3 (Abcam, 1:1000, ab263899), caspase-1 (Abcam, 1:1000, ab179515), Traf3 (Abcam, 1:1000, ab239357), cleaved IL-1β (Cell Signaling Technology, MA, USA, 1:1000, #63124), IL-1β (Abcam, 1:1000, ab283818), and β-actin (Abcam, 1:10000, ab8226) overnight, and hybridized with secondary antibody (Abcam, 1:10000, ab7090) for 60 min. Blots were visualized by GEL imaging system (Bio-Rad, CA, USA) and subsequently analyzed with ImageJ software.

Immunofluorescence of cells

Cells were grown on coverslips or in culture dishes, and after treatment, they were fixed with 4% paraformaldehyde (Sigma-Aldrich) for 20 min at room temperature to preserve cellular structures. After fixation, cells were washed three times with PBS to remove residual fixative. To block nonspecific binding, cells were incubated with 5% bovine serum albumin

for 1 h at room temperature. Following blocking, cells were incubated overnight at 4 °C with the primary antibody against YB-1 (Abcam, 1:100, ab76149). After washing the cells three times with PBS, the cells were then incubated with the corresponding secondary antibody (Abcam, 1:3000, ab150079) for 1 h at room temperature. The secondary antibody was conjugated with a fluorophore, enabling fluorescence detection. To label the cell nuclei, the cells were counterstained with DAPI for 5 min at room temperature. DAPI was used to visualize the nuclei by binding to DNA. After incubation, the cells were washed again with PBS and mounted onto glass slides using an antifade mounting medium. The fluorescence-labeled cells were observed and imaged under a fluorescence microscope (Nikon).

m^{6}A dot blot assay

After denaturation at 65 °C for 5 min, mRNA samples were loaded to an Amersham Hybond-N+ membrane (GE Healthcare, IL, USA) installed in a Bio-Dot Apparatus (Bio-Rad) containing SSC buffer (Sigma-Aldrich). The membrane was UV crosslinked for 5 min followed by washed with PBST. After blocking with 5% nonfat milk, the membrane was incubated with a specific m^{6}A antibody (Abcam, 1:1000, ab284130) overnight at 4 °C. Dot blots were hatched with HRP-conjugated anti-mouse IgG for 1 h before being visualized by an imaging system (Bio-Rad, CA, USA).

Methylated RNA binding protein immunoprecipitation (Me-RIP) assay

Total RNA was extracted from the cells using the TRIzol reagent (ThermoFisher Scientific). The RNA was quantified and assessed for purity using a Nanodrop spectrophotometer (ThermoFisher Scientific). Approximately 1 μg of total RNA was incubated with an m^{6}A antibody (Abcam, 1:500, ab151230) or an IgG antibody (Abcam, 1:100, ab109489) to capture the m^{6}A-modified RNA or the nonspecific binding control, respectively. The reaction mixture was prepared in RIP buffer containing protease inhibitors (Roche, Germany) to prevent RNA degradation. The antibody-RNA complex was then incubated with protein A/G magnetic beads (ThermoFisher Scientific) for 1 h at 4 °C to allow for binding of the antibody to the beads. After incubation, the beads were washed four times with RIP buffer to remove any unbound RNA or nonspecific proteins. Following washing, the RNA-protein complexes were eluted from the beads by adding elution buffer (1% SDS in water) and incubating at 65 °C for 10 min to dissociate the RNA from the beads. The RNA was then extracted using the TRIzol reagent (ThermoFisher Scientific) to remove proteins, and the purified RNA was subjected to qRT-PCR analysis.

ChIP assay

Cells were treated with 1% formaldehyde solution for 10 min, quenched with 125 mM glycine for 5 min and fragmented into 200–500 bp length fragments by sonication. Cell lysate was subsequently incubated with anti-YB-1 (Abcam, 1:30, ab76149) or anti-IgG (Abcam, 1:100, ab211493) at 4 °C overnight. Cross-links for enriching and input DNA were then reversed, and DNA was purified, amplified by PCR and subjected to gel electrophoresis analysis.

Dual-luciferase reporter gene assay

The NLRP3 promoter fragments containing the YB-1 wt/mut binding site were amplified by PCR and inserted into the psiCheck2 vector (Promega, WI, USA) Then, cells were co-transfected with the NLRP3 promoter-wt or NLRP3 promoter-mut and pcDNA3.1 or pcDNA3.1-YB-1. The Luciferase activity was assessed by a dual-luciferase reporter assay system (Promega).

RNA degradation assay

Raw264.7 cells (8×10^4) were incubated with 5 mg/mL actinomycin D (Sigma-Aldrich) for 0 h, 2 h and 4 h. Then RNA was extracted from cells, reverse transcribed to cDNA and examined using qRT-PCR.

RNA pull-down assay

Peli1-sense or anti-sense was transcribed, labeled with biotin (Roche, Mannheim, Germany) and purified. Approximately 2×10^7 cells were dissolved in the soft lysis buffer plus 80 U/mL RNasin (Promega, Madison, WI, USA). The cell extract was incubated with biotinylated RNA for 1 h. Washed streptavidin-coupled agarose beads (Invitrogen) were added to each binding reaction and further incubated for 1 h. Beads were subsequently washed six times in the lysis buffer. The retrieved protein was assessed using western blot.

RIP assay

RIP assay was conducted using a RIP kit (Millipore). Briefly, cells were lysed with a RIP lysis buffer. The cell extract was incubated with IgG (Abcam, 1:50, ab172730) or YTHDC2 (Abcam, 1:30, ab220160) antibodies at 4 °C overnight. RNA was purified from the complex. cDNA was synthesized and used for qRT-PCR assay.

Coimmunoprecipitation (Co-IP)

Cells were lysed in lysis buffer mixed with protease inhibitors. The tissues were homogenized in lysis buffer, and the supernatant was collected by centrifugation. The cell lysate and supernatant were incubated with IgG (Abcam, 1:50, ab172730) or YB-1 (Abcam, 1:30, ab76149) antibodies at 4 °C overnight. Then lysate was incubated with Protein G agarose (Millipore) for 3 h and for the western blot analysis. The ubiquitination of YB-1 was assessed by western blot after obtaining the interacting protein, and the IgG control was included.

Blinding and allocation procedures

During the experiment, randomization was used to allocate animals to the different experimental groups. The randomization sequence was generated using a computer-based random number generator, and the group allocation was initially performed by a researcher who was not involved in any subsequent analysis of the outcomes. The researchers performing the treatments and administering the experimental interventions were blinded to the group allocation at the time of treatment, ensuring that there was no bias in the administration of treatments or procedures. Outcome assessment, including the analysis of tissue samples and measurements, was conducted by investigators who were also blinded to the group allocation. This ensured that the assessment of results, including histological and biochemical analysis, was not influenced by knowledge of the experimental group assignments. For data analysis, the statistical analyses were performed by researchers who were blinded to the group allocation to prevent any bias in the interpretation of the results. Only after the completion of the analysis were the group allocations revealed for interpretation of the results.

Statistics and reproducibility

All data were obtained from three biologically independent experiments for cell culture studies ($n = 3$ independent experiments) and eight biologically independent animals per group for animal studies ($n = 8$ animals/group). The data are expressed as the mean ± standard deviation (SD). Statistical analyses were performed using SPSS 19.0 software. For comparisons between two groups, the Student's t-test was used. For comparisons between multiple groups, one-way ANOVA was performed. In the case of significant differences, post hoc tests were used to further analyze the data. A p-value of less than 0.05 was considered statistically significant. For all statistical tests, the effect size was calculated to estimate the magnitude of the observed differences, and the corresponding 95% confidence intervals were included when applicable. Where applicable, statistical tests were chosen based on the nature of the data, and assumptions of normality were tested using appropriate tests (Shapiro-Wilk test) prior to the analysis.

Reporting summary

Further information on research design is available in the Nature Portfolio Reporting Summary linked to this article.

Data availability

All data generated or analyzed in this study are included in the manuscript and Supplementary Information file. The file of Supplementary Data contains the underlying numerical source data for the study.

Abbreviations

AS	Atherosclerosis
NLRP3	Nucleotide-binding domain (NOD)-like receptor (NLR) family member pyrin domain-containing protein 3
ASC	Apoptosis-associated speck-like protein
IL	Interleukin
YB-1	Y-box binding protein 1
VSMC	Vascular smooth muscle cell
Peli1	Pellino 1
ox-LDL	Oxidized low-density lipoprotein
m^6A	N6-methyladenosine
METTL3	Methyltransferase-like 3
YTHDC2	YTH domain-containing 2
TC	Total cholesterol
TG	Triglyceride
HDLC	High-density lipoprotein cholesterol
LDLC	Low-density lipoprotein cholesterol
HE	Hematoxylin-eosin
ELISA	Enzyme-linked immunosorbent assay
Me-RIP	Methylated RNA binding protein immunoprecipitation
HE	Hematoxylin-eosin
Co-IP	Coimmunoprecipitation
RIP	RNA immunoprecipitation
qRT-PCR	Quantitative real-time polymerase chain reaction
SD	Standard deviation
ANOVA	Analysis of variance

Received: 31 July 2023; Accepted: 27 February 2025;
Published online: 19 March 2025

References

1. Zhang, X. et al. Desmosterol suppresses macrophage inflammasome activation and protects against vascular inflammation and atherosclerosis. *Proc. Natl Acad. Sci. USA* **118**, e2107682118 (2021).
2. Kotla, S., Singh, N. K. & Rao, G. N. ROS via BTK-p300-STAT1-PPARγ signaling activation mediates cholesterol crystals-induced CD36 expression and foam cell formation. *Redox Biol.* **11**, 350–364 (2017).
3. Quillard, T., Croce, K., Jaffer, F. A., Weissleder, R. & Libby, P. Molecular imaging of macrophage protease activity in cardiovascular inflammation in vivo. *Thromb. Haemost.* **105**, 828–836 (2011).
4. Xu, Q. et al. The role of the inflammasomes in the pathogenesis of uveitis. *Exp. Eye Res.* **208**, 108618 (2021).
5. Duewell, P. et al. NLRP3 inflammasomes are required for atherogenesis and activated by cholesterol crystals. *Nature* **464**, 1357–1361 (2010).
6. Tall, A. R. & Westerterp, M. Inflammasomes, neutrophil extracellular traps, and cholesterol. *J. Lipid Res.* **60**, 721–727 (2019).
7. Meyer, N. et al. Y-box binding protein 1 expression in trophoblast cells promotes fetal and placental development. *Cells* **9**, 1942 (2020).
8. Lyabin, D. N., Eliseeva, I. A. & Ovchinnikov, L. P. YB-1 protein: functions and regulation. *Wiley Interdiscip. Rev. RNA* **5**, 95–110 (2014).
9. Hanssen, L. et al. Y-box binding protein-1 mediates profibrotic effects of calcineurin inhibitors in the kidney. *J. Immunol.* **187**, 298–308 (2011).
10. Bernhardt, A. et al. Inflammatory cell infiltration and resolution of kidney inflammation is orchestrated by the cold-shock protein Y-box binding protein-1. *Kidney Int.* **92**, 1157–1177 (2017).
11. Shi, J. H. et al. Novel insight into Y-box binding protein 1 in the regulation of vascular smooth muscle cell proliferation through targeting GC box-dependent genes. *FEBS Lett.* **587**, 1326–1332 (2013).
12. Wang, F. et al. Soyasaponin II protects against acute liver failure through diminishing YB-1 phosphorylation and Nlrp3-inflammasome priming in mice. *Theranostics* **10**, 2714–2726 (2020).
13. Hu, H. & Sun, S. C. Ubiquitin signaling in immune responses. *Cell Res.* **26**, 457–483 (2016).
14. Liu, J. et al. Peli1 negatively regulates noncanonical NF-κB signaling to restrain systemic lupus erythematosus. *Nat. Commun.* **9**, 1136 (2018).
15. Burger, F., Baptista, D., Roth, A., Brandt, K. J. & Miteva, K. The E3 ubiquitin ligase Peli1 deficiency promotes atherosclerosis progression. *Cells* **11**, 2014 (2022).
16. Roundtree, I. A., Evans, M. E., Pan, T. & He, C. Dynamic RNA modifications in gene expression regulation. *Cell* **169**, 1187–1200 (2017).
17. Zheng, Y, et al. Mettl14 mediates the inflammatory response of macrophages in atherosclerosis through the NF-κB/IL-6 signaling pathway. *Cell. Mol. Life Sci.* **79**, 311 (2022).
18. Jian, D. et al. METTL14 aggravates endothelial inflammation and atherosclerosis by increasing FOXO1 N6-methyladeosine modifications. *Theranostics* **10**, 8939–8956 (2020).
19. Dong, G. et al. N6-methyladenosine methyltransferase METTL3 promotes angiogenesis and atherosclerosis by upregulating the JAK2/STAT3 pathway via m6A reader IGF2BP1. *Front. Cell Dev. Biol.* **9**, 731810 (2021).
20. Johnston, J. M. et al. Myeloid Tribbles 1 induces early atherosclerosis via enhanced foam cell expansion. *Sci. Adv.* **5**, eaax9183 (2019).
21. Wang, X. et al. WWP2 ameliorates oxidative stress and inflammation in atherosclerotic mice through regulation of PDCD4/HO-1 pathway. *Acta Biochim. Biophys. Sin.* **54**, 1057–1067 (2022).
22. Wang, Z. C. et al. A dual Keap1 and p47(phox) inhibitor Ginsenoside Rb1 ameliorates high glucose/ox-LDL-induced endothelial cell injury and atherosclerosis. *Cell Death Dis.* **13**, 824 (2022).
23. Galbas, T. et al. MARCH1 E3 ubiquitin ligase dampens the innate inflammatory response by modulating monocyte functions in mice. *J. Immunol.* **198**, 852–861 (2017).
24. Kotla, S. et al. Endothelial senescence-associated secretory phenotype (SASP) is regulated by Makorin-1 ubiquitin E3 ligase. *Metab. Clin. Exp.* **100**, 153962 (2019).
25. Zeng, C., Huang, W., Li, Y. & Weng, H. Roles of METTL3 in cancer: mechanisms and therapeutic targeting. *J. Hematol. Oncol.* **13**, 117 (2020).
26. Hsu, P. J. et al. Ythdc2 is an N6-methyladenosine binding protein that regulates mammalian spermatogenesis. *Cell Res*. **27**, 1115–1127 (2017).
27. Mo, H. et al. Decreased Peli1 expression attenuates osteoarthritis by protecting chondrocytes and inhibiting M1-polarization of macrophages. *Bone Jt. Res.* **12**, 121–132 (2023).
28. Libby, P., Ridker, P. M. & Hansson, G. K. Progress and challenges in translating the biology of atherosclerosis. *Nature* **473**, 317–325 (2011).
29. Kelley, N., Jeltema, D., Duan, Y. & He, Y. The NLRP3 inflammasome: an overview of mechanisms of activation and regulation. *Int. J. Mol. Sci.* **20**, 3328 (2019).
30. Hoseini, Z. et al. NLRP3 inflammasome: its regulation and involvement in atherosclerosis. *J. Cell. Physiol.* **233**, 2116–2132 (2018).
31. Raffetseder, U., Liehn, E. A., Weber, C. & Mertens, P. R. Role of cold shock Y-box protein-1 in inflammation, atherosclerosis and organ transplant rejection. *Eur. J. Cell Biol.* **91**, 567–575 (2012).
32. Krohn, R. et al. Y-box binding protein-1 controls CC chemokine ligand-5 (CCL5) expression in smooth muscle cells and contributes to neointima formation in atherosclerosis-prone mice. *Circulation* **116**, 1812–1820 (2007).

33. Zhou, Z. X. et al. The role of ubiquitin E3 ligase in atherosclerosis. *Curr. Med. Chem.* **28**, 152–168 (2021).
34. Cockram, P. E. et al. Ubiquitination in the regulation of inflammatory cell death and cancer. *Cell Death Differ.* **28**, 591–605 (2021).
35. Zhang, L. et al. Peli1 facilitates NLRP3 inflammasome activation by mediating ASC ubiquitination. *Cell Rep.* **37**, 109904 (2021).
36. Fu, J. et al. The role of m6A ribonucleic acid modification in the occurrence of atherosclerosis. *Front. Genet.* **12**, 733871 (2021).
37. Robinson, M., Shah, P., Cui, Y. H. & He, Y. Y. The role of dynamic m6A RNA methylation in photobiology. *Photochem. Photobiol.* **95**, 95–104 (2019).
38. Xu, B, et al. Mettl3-mediated m6A modification of Lrp2 facilitates neurogenesis through Ythdc2 and elicits antidepressant-like effects. *FASEB J.* **36**, e22392 (2022).
39. Miano, J. M., Fisher, E. A. & Majesky, M. W. Fate and state of vascular smooth muscle cells in atherosclerosis. *Circulation* **143**, 2110–2116 (2021).
40. Grootaert, M. O. J. & Bennett, M. R. Vascular smooth muscle cells in atherosclerosis: time for a re-assessment. *Cardiovasc. Res.* **117**, 2326–2339 (2021).
41. Bennett, M. R., Sinha, S. & Owens, G. K. Vascular smooth muscle cells in atherosclerosis. *Circ. Res.* **118**, 692–702 (2016).

Acknowledgements

This work was supported by the National Natural Science Foundation of China (General Program 82160093 and 82360145).

Author contributions

Qiang Liu conceived the ideas, designed the experiments, and wrote the manuscript. Lu Yan also conceived the ideas, designed the experiments, and performed the experiments. Tao Wu performed the experiments, analyzed the data, and contributed to the writing of the manuscript. Qinghua Wu analyzed the data and provided critical feedback on the manuscript. Ben Ke provided critical materials, supervised the study, and contributed to the manuscript revision. Wen Shen wrote the manuscript and supervised the overall study. All authors have read and approved the final version of the manuscript for publication.

Competing interests

The authors declare no competing interests.

Ethical approval

The animal studies were approved by the Second Affiliated Hospital of Nanchang University (Review [2023] No. (323)).

Additional information

Supplementary information The online version contains supplementary material available at https://doi.org/10.1038/s42003-025-07839-w.

Correspondence and requests for materials should be addressed to Ben Ke or Wen Shen.

Peer review information *Communications Biology* thanks Sivareddy Kotla, Kapka Miteva and the other anonymous reviewer(s) for their contribution to the peer review of this work. Primary handling editor: Johannes Stortz.